Geochemical Perspectives Letters

Chondritic chlorine isotope composition of acapulcoites and lodranites

A. Stephant, M. Anand, C. Carli, X. Zhao, J. Davidson, T. Cuppone, G. Pratesi, I.A. Franchi

Supplementary Information

The Supplementary Information includes:

- Sample description
- Mineralogical and petrological analyses
- Chlorine abundance and isotopic composition analyses
- Tables S-1 and S-2
- Figures S-1 to S-5
- Supplementary Information References

Sample description

Acapulco

Acapulco fell on August 11, 1976 in Mexico and was first studied by Christophe Michel-Levy and Lorin (1978). In addition to being a fall, Acapulco is relatively unshocked (S1) (Palme *et al.,* 1981), similar to many other acapulcoites and lodranites. Acapulco is mostly composed of silicate minerals: olivine (25.1 vol. %), pyroxene, mostly as orthopyroxene (44 vol. %), feldspar (15 vol. %) (Yugami *et al.,* 1998). Using XMapTools 4.1 (Lanari *et al.,* 2014; 2019; 2023), we recalculated similar modal abundances for Acapulco (vol. %): 27.3 of olivine, 50.1 of orthopyroxene, 0.3 of clinopyroxene, 9.8 of feldspar, 10.9 of metallic phases and 1.6 of Ca-phosphates. Zipfel *et al.* (1995) reported no zoning in MgO and FeO in these silicates, consistent with this sample probably being the most equilibrated acapulcoite (McCoy *et al.,* 1996). Acapulco yields a higher metamorphism temperature than type 5–6 ordinary chondrites (Zipfel *et al.,* 1995), with an estimated temperature of 1170 °C (McCoy *et al.,* 1996; Palme *et al.,* 1981). McCoy *et al.* (1997b) estimated that Acapulco suffered from less than 1 % partial melting. In Acapulco, apatite is much more abundant than merrillite. A vein of Cl-F-bearing apatite in Acapulco was 1.8 mm *vs*. 200 microns in size (McCoy *et al.,* 1996).

NWA 10074

Northwest Africa (NWA) 10074 is an acapulcoite classified in 2014. It shows a recrystallized texture, with polygonal and subhedral grains typically <0.3 mm, with occasional larger (to 1 mm) grains of orthopyroxene. Silicates have homogenous compositions and represent 90 vol. % of the sample but no

precise modal abundances have yet been reported. We estimated modal abundances as follow (vol. %): 28.4 of olivine, 40.5 of orthopyroxene, 4.5 of clinopyroxene, 14 of feldspar, 7 of metallic phases and 0.5 of Ca-phosphates. The shock and weathering grades of this sample are low.

Dhofar 125

Dhofar 125 is another acapulcoite, found in 2000 in the Oman desert. Dhofar 125 is moderately weathered (W1) in the interior core of the rock, while slightly more weathered (W2) towards the edges. As for other acapulcoites, Dhofar 125 is dominated by orthopyroxene (35.6 vol. %), olivine (27.5 vol. %), feldspar (14 vol. %) and clinopyroxene (6.5 vol. %) (Greyshake *et al.,* 2001). Recalculated modal abundances using XMapTools 4.1 are consistent with these previous estimations (vol. %): 28.4 of olivine, 36.5 of orthopyroxene, 6.1 of clinopyroxene, 5.9 of feldspar, 22.5 of metallic phases and 0.3 of Ca-phosphates. The meteorite is also unshocked, similar to most other acapulcoites and lodranites, with olivine showing sharp extinction and few irregular fractures. Dhofar 125 also shows recrystallized texture with abundant 120° triple junctions (Patzer *et al.,* 2004), but its average grain size (97.3 μm) is slightly smaller than typical acapulcoites. Its equilibration temperature has been estimated at 1120 °C (Patzer *et al.,* 2004).

Lodran

Lodran fell in 1868 in Pakistan and is also unshocked (Sl) (McCoy *et al*., 1997a). Conversely to Acapulco, Lodran exhibits evidence for more than 20% of partial melting (Papike *et al.,* 1995). Based on the modal abundance data of Davis *et al.* (1993), Lodran is comprised of 53 vol. % of olivine and 47 vol. % of orthopyroxene, with some trace of chromite. Our thin section sample contains some large blebs of Fe-Ni metal compared to the one studied by Davis *et al.* (1993). Using XMapTools 4.1, we recalculated the modal abundances of Lodran (vol. %): 41.3 of olivine, 36.4 of orthopyroxene, 22.2 of metallic phases and 0.07 of Ca-phosphates.

NWA 11970

Northwest Africa 11970 was classified in 2016 as one of the few lodranite breccias. This material is likely paired with NWA 8118, NWA 8216, and NWA 8251. The weathering grade is also very low. Observations from a thin section show a breccia dominated by angular to sub-rounded silicate grains of which the largest grain is 1 cm long. Mineralogy is dominated by olivine, ortho- and clinopyroxenes. Estimations from XMapTools give modal abundances (vol. %) of 48.7 of olivine, 18.7 of clinopyroxene, 26.1 of orthopyroxene, 0.1 of phosphates and 6.9 of metallic phases.

Mineralogical and petrological analyses

Backscattered electron (BSE) images were obtained on polished thin sections of acapulcoites and lodranites loaned from the Buseck Center for Meteorite Studies (BCMS). Elemental X-ray maps of Ca, Fe, Mg, P and Si were collected on the Cameca SX-100 electron probe microanalyser (EPMA) at University of Arizona to identify Ca-phosphates in thin sections of Acapulco, NWA 10074, Dhofar 125, Lodran and NWA 11970 (Fig. S-1). Chemical characterisation of Ca-phosphates in these thin sections, performed after NanoSIMS analyses to avoid devolatilization, was carried out with a JEOL Superprobe JXA-8230 EMPA at the Department of Earth Sciences, University of Firenze. Quantitative analyses of Ca-phosphates were performed in wavelength dispersive mode, with an accelerating potential of 15 kV. A focused beam of 20 nA with a 3 μm spot size was used. ZAF correction was applied to all measurements. Typical detection limits were 0.02–0.05 % for major element oxide abundances. Standards used for these analyses are: albite astimex for Na, apatite astimex for P and Ca, fluorine

astimex for F, celestite astimex for Sr, tugtupite astimex for Cl, ilmenite from the Smithsonian for Fe, olivine astimex for Mg. Crystals for element detection were TAP for Na and Mg, PET for P, Sr, Cl and Ca, LIF for Fe and LDE1 for F. As F−, Cl−, and hydroxyl (OH−) anions occupy the X crystallographic site, Cl and F concentrations were corrected for apatite stoichiometry assuming $2 = X_F + X_{Cl} + X_{OH}$, following the method of Ketcham (2015). Since these Ca-phosphates are dry (<50 $\mu g.g^{-1}$ H_2O) (Stephant *et al*., 2023) and that Cl contents measured by NanoSIMS and by EPMA are consistent, it is most likely that F content by EPMA is overestimated, as also suggested by McCubbin *et al.* (2021). The chemical compositions of Ca-phosphates are presented in supplementary Table S-1. Modal abundances and estimation of bulk F, Cl and H_2O abundances in the studied samples following the method described in McCubbin *et al.* (2021) is provided in supplementary Table S-2.

Chlorine abundance and isotopic composition analyses

Chlorine abundances and Cl-isotopic compositions of 15 apatite were measured using the Cameca NanoSIMS 50L at the Open University, UK using a protocol modified after Tartèse *et al.* (2014), Barnes *et al.* (2016) and Barrett *et al.* (2019) following two modes: spot analyses for larger apatite grains found in Acapulco, NWA 10074 and Dhofar 125 (Ph3, Ph4 and Ph5) and imaging for grains which were less than 50 µm diameter in Lodran, NWA 11970 and Dhofar 125 (Ph 1 and Ph2) (cf. Supplementary Fig. S-2). For spot analyses, $^{1}H^{16}O$, ^{18}O, ^{35}Cl, ^{37}Cl, $^{40}Ca^{19}F$ secondary ions were measured using a Cs^+ primary beam of 10 pA rastered over 5 µm × 5 µm surface area. Each analysis surface area was divided into 64 × 64 pixels, with a counting time of 0.132 ms per pixel. The number of cycles was set at 800. Three minutes of pre-sputtering was set-up before analysis on a larger area (7 µm × 7 µm) than the analysed surface to remove any contamination from the surface and establish sputter equilibrium. An electron flood gun was used for charge compensation. $^{40}Ca^{19}F$ secondary ions were used to monitor that the spot was within the apatite. For image mode, the same secondary negative electrons were imaged by scanning ion imaging. Analyses were carried out using a Cs^+ primary current of 10 pA that was rastered over the sample on areas of 10 µm × 10 µm. Each analysis surface area was divided into 128 ×128 pixels, with a counting time of 1 ms per pixel. The number of cycles was set at 100. Pre-sputtering (15 µm × 15 µm) was also set-up before analysis, as well as the use of the electron flood gun. Images were processed with the L'IMAGE software developed by Larry Nittler from the Carnegie Institute of Washington (now Arizona State University). The deadtime was set at 44 ns and corrected with the L'IMAGE software. Regions of interest (ROIs) were determined on each image based on the $^{35}Cl/^{18}O$ and $^{40}Ca/^{18}O$ images to locate the apatite and exclude any cracks, voids or anomalously Cl-rich hotspots associated with extraneous contamination.

For both sets of analyses, terrestrial apatite standards Ap 004, Ap 005 and Ap 018 were used for relative sensitivity factor of Cl abundance (McCubbin *et al.,* 2012). Cl abundances were calibrated using the measured $^{35}Cl/^{18}O$ ratios and the known Cl abundances of terrestrial apatite standards (Fig. S-3). Uncertainties reported on Cl contents combine the 2σ analytical uncertainties associated with each individual measurement and the uncertainty associated with the calibration line. The good match between NanoSIMS and EPMA Cl content values give credit to the accuracy of our NanoSIMS analyses (Fig. S-4).

For Cl isotope measurements, the instrumental mass fractionation (IMF) factor, α, based on analyses of Ap 005 was 1.028 ± 0.001 (2s.d.) for spot analyses and 1.016 ± 0.001 (2s.d.) for image mode.

Reproducibility of $\delta^{37}Cl$ measurements on Ap 005 standard is presented in Figure S-4. The measured $^{37}Cl/^{35}Cl$ ratios are corrected for the IMF and expressed in $\delta^{37}Cl$ notation as defined in equation (Eq. S-1), with standard mean ocean chloride $\delta^{37}Cl_{SMOC}=0$ (Kaufman *et al.*, 1984).

$$\delta^{37}Cl\ (‰) = [(^{37}Cl/^{35}Cl_{sample})/(^{37}Cl/^{35}Cl_{SMOC})–1] \times 1000 \quad \text{(Eq. S-1)}$$

Weighted average of Ap 004 $\delta^{37}Cl$, corrected from IMF, is 0.27 ± 0.23 ‰ (N=33), consistent with its published value of 0.11 ‰ (McCubbin *et al.,* 2012). Errors estimated for $\delta^{37}Cl$ values take into consideration the error based on counting statistics, as well as the uncertainty associated with the IMF calculation. BSE images of analysed apatite and optical images of NanoSIMS spots can be found in Figure S-5.

Supplementary Tables

Table S-1 Chemical composition of apatite and merrillites in Acapulco, NWA 10074, Dhofar 125, Lodran and NWA 11970. Merri. Stands for merrillite. Data were processed using the "approach 1" template in Ketcham (2015). We assume that OH = 2 – (X_F and X_{Cl}) when the sum of X_F and X_{Cl} was below 2. When the sum of X_F and X_{Cl} exceeds 2 afu, F was computed assuming $X_F = 2 – X_{Cl}$. This is because F can be overestimated by EMPA (Davidson *et al.,* 2020; McCubbin *et al*., 2021), as highlighted by the fit between Cl abundance measured by EPMA and SIMS (cf. Figure S-5). Table S-1 (.xlxs) is available for download from the online version of this article at https://doi.org/10.7185/geochemlet.2406

Table S-2 Modal abundances of Acapulco, NWA 10074, Dhofar 125 and Lodran, from literature and this study, with the estimation of bulk F, H_2O and Cl abundances, based on the partition coefficient between melt and apatite of F, Cl and OH from McCubbin *et al.* (2015) and the method described in McCubbin *et al.* (2021). Apatite H_2O contents from Stephant *et al. (*2023) were used to calculate H_2O /F ratios. Literature data are given for comparison.

	Acapulco		NWA 10074	Dhofar 125		Lodran
Olivine	25.2	27.3	28.4	27.5	28.5	41.28
High-Ca pyroxene	2.5	0.3	4.5	6.5	6.1	
Low-Ca pyroxene	41.1	50.1	40.5	35.6	36.7	36.44
Plagioclase	14.8	9.8	14	14	5.9	
Chromite	0.8	-		0.5	-	
Ca-phosphate	1.2	1.6	0.5	0.7	0.3	0.07
Troilite	8.7	-	7	7.7	-	
Metal	5.7	10.9	3	5.3	22.5	22.21
Total	100.0	100	97.9	97.8	99.9	100
Reference	*Yugami et al. (1998)*	*This study*	*This study*	*Greyshake et al. (2001)*	*This study*	*This study*

Table S-2 continued	Acapulco		NWA 10074	Dhofar 125		Lodran
F wt.% in apatite	2.82 ± 0.09		3.55 ± 0.14	0.69 ± 0.22 (75% of apatite) 2.26 (25% of apatite)		0.37 ± 0.03
F bulk rock (mg.g^{-1}) this study	**308**	**392**	**171**	**71**	**42**	**2**
error	**±10**	**±10**	**±10**	**±10**	**±10**	**±0.1**
H_2O/F	0.037 - 0.077		0.015 - 0.052	0.180		
Cl/F	0.98 - 1.28		0.28 - 0.32	2.56 – 26.34		29.43 – 36.25
H_2O bulk (µg.g^{-1}) this study	**11-24**	**14 - 30**	**03-09**	**< 27**	**< 9**	
H_2O bulk (µg.g^{-1}) (Stephant *et al.*, 2023)	03-09		06-18	05-14		18 - 31
Cl bulk (µg.g^{-1}) lower limits - this study	**302 - 394**	**384 - 501**	**47 - 54**	**374 – 1185**	**131-421**	**59- 73**
Cl bulk (µg.g^{-1}) (McCoy *et al.*, 1997b)	250					10
Cl bulk (µg.g^{-1}) (Garrison *et al.*, 2000)	204 ± 246		131 - 268*	131 - 268*		35 - 78*

* range of average values

Supplementary Figures

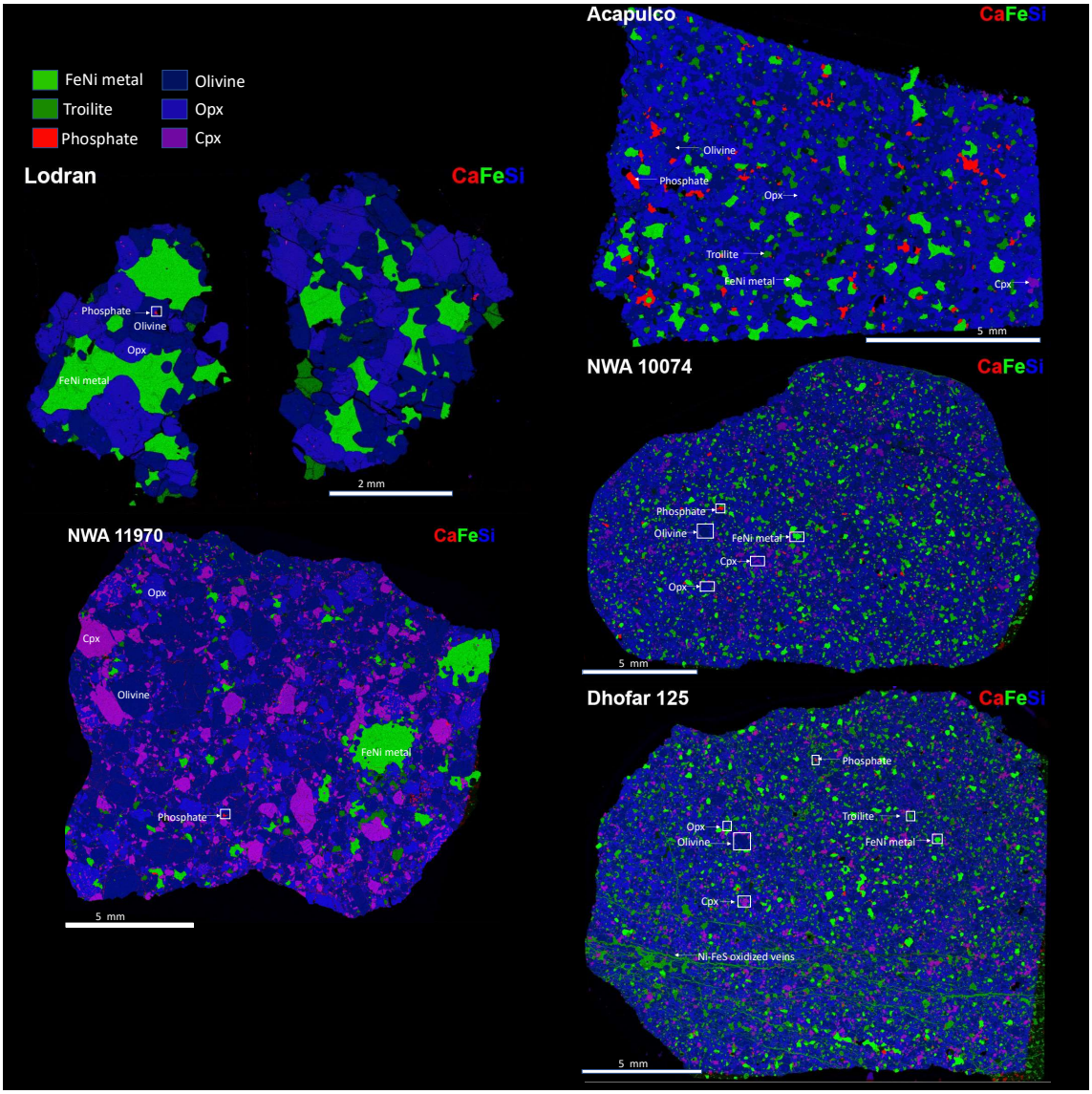

Figure S-1 Composite X-ray maps of Acapulco, NWA 10074, Dhofar 125, Lodran and NWA 11970 showing the distribution of FeNi metal, troilite, olivine, orthopyroxene (opx), clinopyroxene (cpx) and Ca-phosphates. Ca-phosphates in acapulcoites are generally associates with FeNi metal, while they are bounded to silicates in lodranites. Acapulco exhibit large grains of apatite of a few hundreds of microns, while acapulcoite apatite size range from 50 to 200 microns. Lodranites display apatite grains smaller than 50 microns in size.

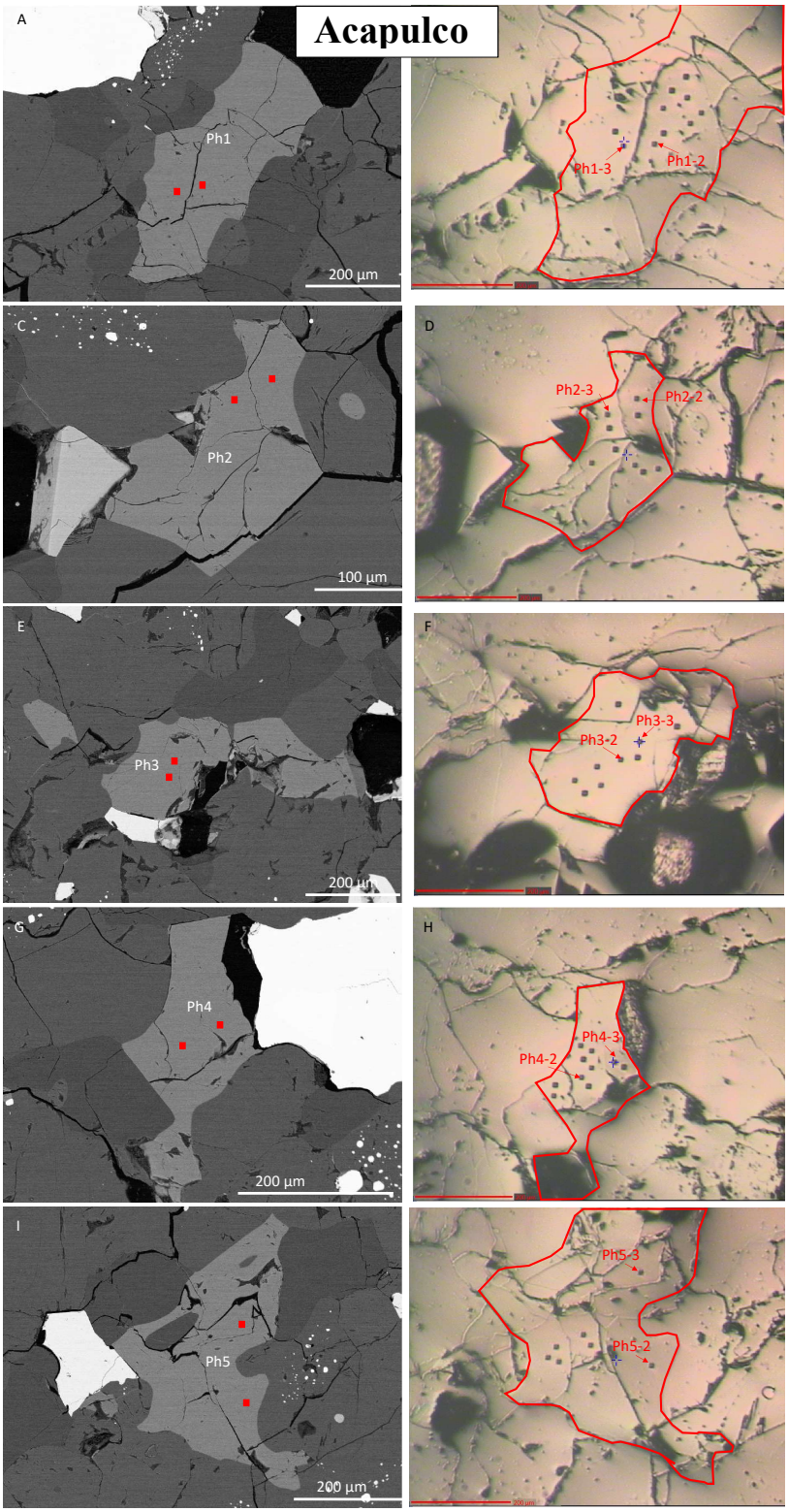
Acapulco
A
Ph1
200 µm
Ph1-3
Ph1-2
C
Ph2
100 µm
D
Ph2-3
Ph2-2
E
Ph3
200 µm
F
Ph3-3
Ph3-2
G
Ph4
200 µm
H
Ph4-3
Ph4-2
I
Ph5
200 µm
Ph5-3
Ph5-2

Figure S-2

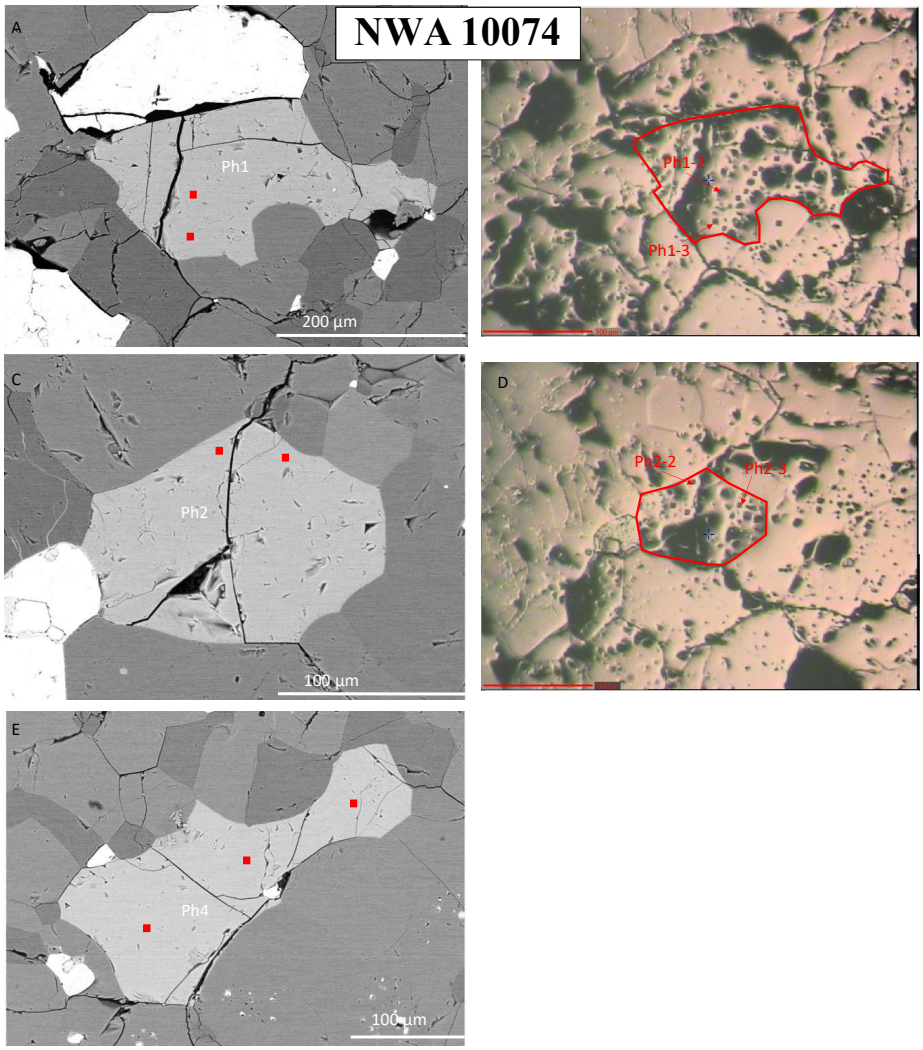

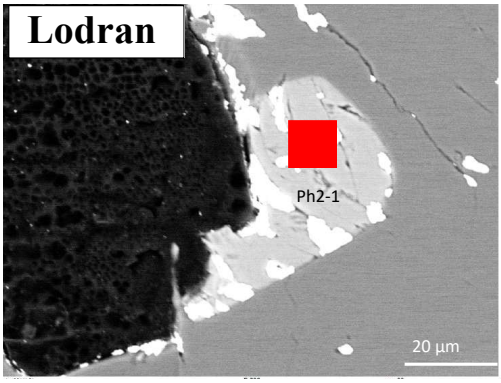

Figure S-2 *continued*

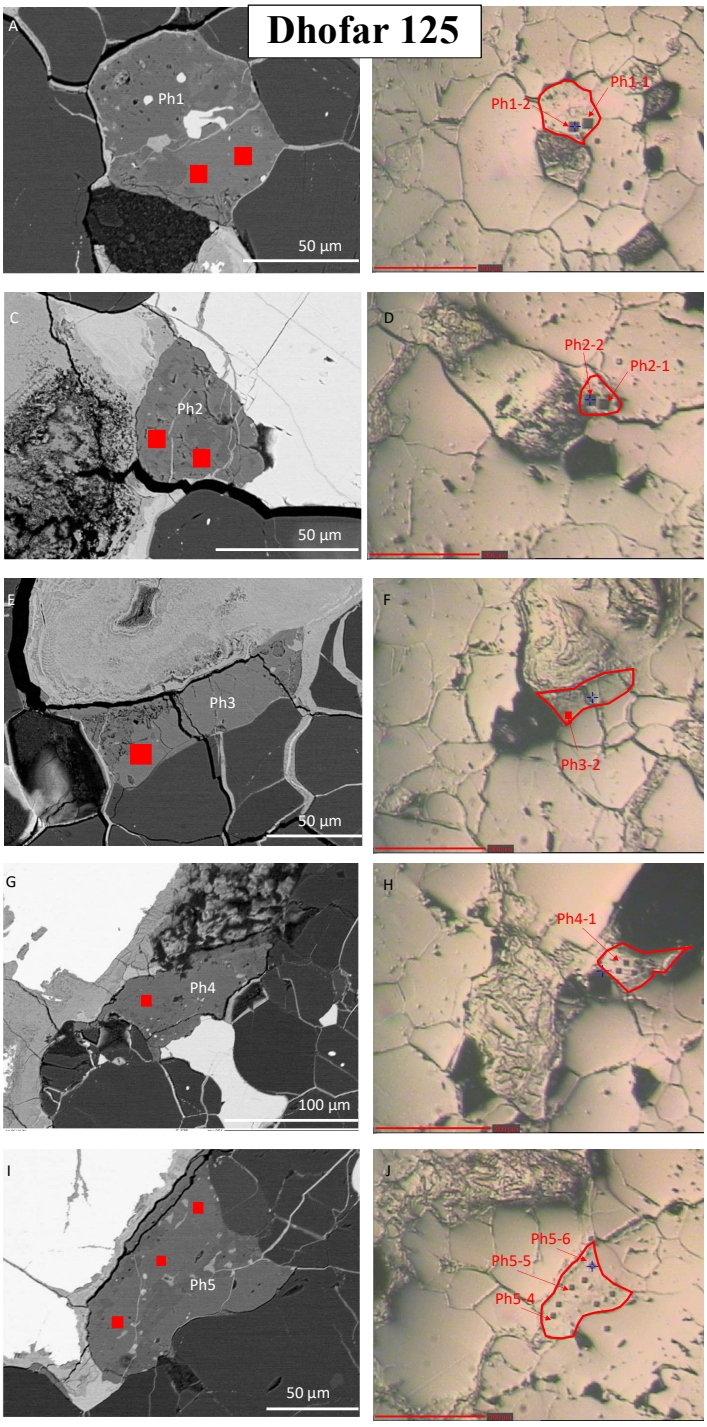

Figure S-2 BSE images of apatite and associated optical images highlighting the NanoSIMS spots. Extra spots appearing on the optical images were made for analytical settings and during hydrogen analyses (Stephant *et al.,* 2023).

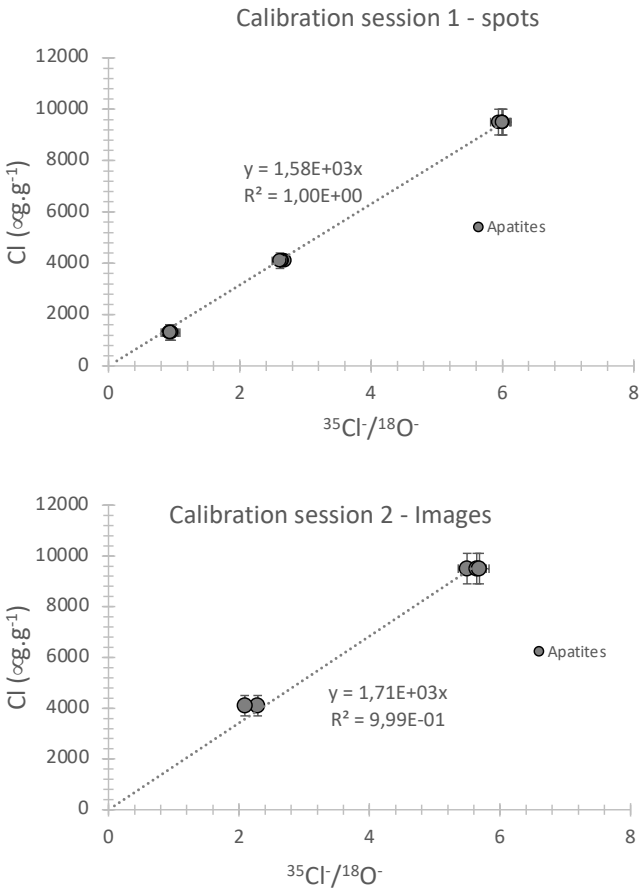

Figure S-3 Calibration curves for determination of chlorine abundance (μg.g^{-1}) as a function of $^{35}Cl^{-}/^{18}O^{-}$ measured by NanoSIMS based on terrestrial apatite standards.

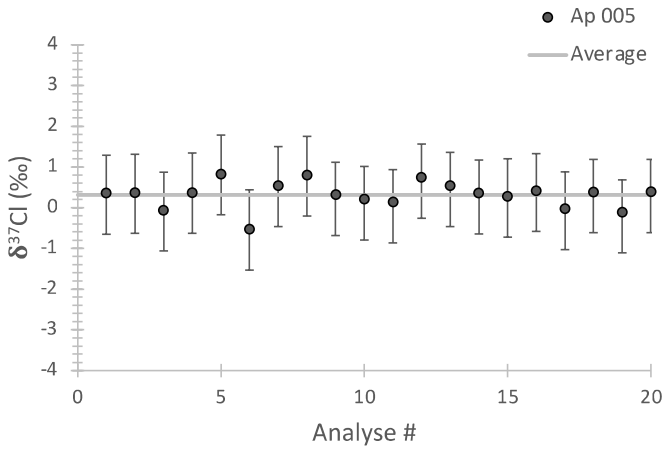

Figure S-4 Reproducibility of $\delta^{37}Cl$ in Apatite 005 standard over the duration of the analysis session. The error bars represent the analytical error associated within each measurement. Grey band represent the average $\delta^{37}Cl$ value of the standard.

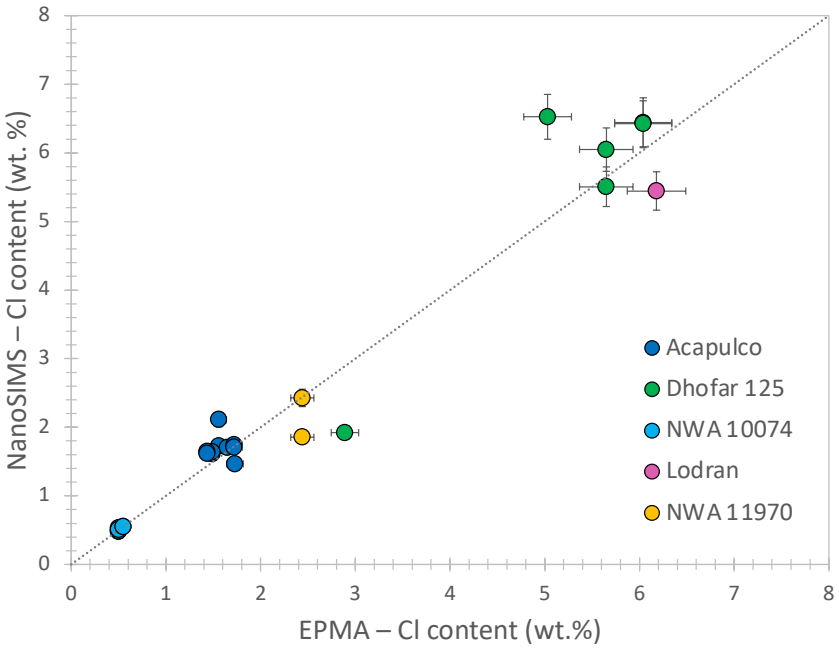

Figure S-5 EPMA *vs*. SIMS Cl abundances (wt. %) in acapulcoites and lodranites.

Supplementary Information References

Barnes, J.J., Tartèse, R., Anand, M., McCubbin, F.M., Neale, C.R., Franchi, I.A. (2016) Early degassing of lunar urKREEP by crust-breaching impact(s). *Earth and Planetary Science Letters* 447, 84–94. https://doi.org/10.1016/j.epsl.2016.04.036

Barrett, T.J., Barnes, J.J., Anand, M., Franchi, I.A., Greenwood, R.C., Charlier, B.L.A., Zhao, X., Moynier, F., Grady, M.M. (2019) Investigating magmatic processes in the early Solar System using the Cl isotopic systematics of eucrites. *Geochimica et Cosmochimica Acta* 266, 582–597. https://doi.org/10.1016/j.gca.2019.06.024

Christophe Michel-Levy, M., Lorin, J.C. (1978) El quemado, a new type of stone meteorite fallen near Acapulco (Abstract). *Meteoritics* 13, 411–412.

Davidson, J., Wadhwa, M., Hervig, R.L., Stephant, A. (2020) Water on Mars: Insights from apatite in regolith breccia Northwest Africa 7034. *Earth and Planetary Science Letters* 552, 116597. https://doi.org/10.1016/j.epsl.2020.116597

Davis, A.M., Prinz, M., Weisberg, M.K. (1993) Trace Element Distributions in Primitive Achondrites, *Lunar and Planetary Science Conference XXIV* 375-376, The Woodlands, Texas.

Garrison, D., Hamlin, S., Bogard, D. (2000) Chlorine abundances in meteorites. *Meteoritics and Planetary Science* 35, 419-429. https://doi.org/10.1111/j.1945-5100.2000.tb01786.x

Greyshake, A., Clayton, R.N., Mayeda, T.K. (2001) Dhofar 125: A new acapulcoite from Oman. *Lunar and Planetary Science Conference XXXII* #1325, The Woodlands, Texas.

Kaufman, R., Long, A., Bentley, H., Davis, S. (1984) Natural chlorine isotope variations. *Nature* 309, 338–340. https://doi.org/10.1038/309338a0

Ketcham, R.A. (2015) Technical Note: Calculation of stoichiometry from EMP data for apatite and other phases with mixing on monovalent anion sites. *American Mineralogist* 100, 1620–1623. https://doi.org/10.2138/am-2015-5171

Lanari, P., Vidal, O., De Andrade, V., Dubacq, B., Lewin, E., Grosch, E., Schwartz, S. (2014) XMapTools: a MATLAB©-based program for electron microprobe X-ray image processing and geothermobarometry. *Computers and Geosciences* 62, 227-240. https://doi.org/10.1016/j.cageo.2013.08.010

Lanari, P., Vho, A., Bovay, T., Airaghi, L., Centrella, S., (2019) Quantitative compositional mapping of mineral phases by electron probe micro-analyser. *Geological Society of London*, Special Publications 478, 39-63. https://doi.org/10.1144/SP478.4

Lanari, P., Laughton, J., Tedeschi, M., Markmann, T.A. (2023) XMapTools 4.1 (v4.1). *Zenodo.* https://doi.org/10.5281/zenodo.7656958

McCoy, T.J., Keil, K., Clayton, R.N., Mayeda, T.K., Bogard, D.D., Garrison, D.H., Huss, G.R., Hutcheon, I.D., Wieler, R. (1996) A petrologic, chemical, and isotopic study of Monument Draw and comparison with other acapulcoites: Evidence for formation by incipient partial melting. *Geochimica et Cosmochimica Acta* 60, 2681–2708. https://doi.org/10.1016/0016-7037(96)00109-3

McCoy, T.J., Keil, K., Clayton, R.N., Mayeda, T.K., Bogard, D.D., Garrison, D.H., Wieler, R. (1997a) A petrologic and isotopic study of lodranites: Evidence for early formation as partial melt residues from heterogeneous precursors. *Geochimica et Cosmochimica Acta* 61, 623–637. https://doi.org/10.1016/S0016-7037(96)00359-6

McCoy, T.J., Keil, K., Muenow, D.W., Wilson, L. (1997b) Partial melting and melt migration in the acapulcoite-lodranite parent body. *Geochimica et Cosmochimica Acta* 61, 639–650. https://doi.org/10.1016/S0016-7037(96)00365-1

McCubbin, F.M., Hauri, E.H., Elardo, S.M., Vander Kaaden, K.E., Wang, J., Shearer Jr, C.K. (2012) Hydrous melting of the martian mantle produced both depleted and enriched shergottites. *Geology* 40, 683-686. https://doi.org/10.1130/G33242.1

McCubbin F.M., Vander Kaaden K.E., Tartèse R., Boyce J.W., Mikhail S., Whitson E.S., Bell A.S., Anand M., Franchi I.A., Wang J.H., Hauri E.H. (2015) Experimental investigation of F, Cl, and OH partitioning between apatite and Fe-rich basaltic melt at 1.0-1.2 GPa and 950-1000 °C. *American Mineralogist* 100, 1790-1802. https://doi.org/10.2138/am-2015-5233

McCubbin, F.M., Lewis, J.A., Barnes, J.J., Elardo, S.M., Boyce J.W. (2021). The abundances of F, Cl, and H_2O in eucrites: Implications for the origin of volatile depletion in the asteroid 4 Vesta. *Geochimica et Cosmochimica Acta* 314, 270-293. https://doi.org/10.1016/j.gca.2021.08.021

Palme, H., Schultz, L., Spettel, B., Weber, H.W., Wänke, H., Michel-Levy, M.C., Lorin, J.C. (1981). The Acapulco meteorite: Chemistry, mineralogy and irradiation effects. *Geochimica et Cosmochimica Acta* 45, 727–752. https://doi.org/10.1016/0016-7037(81)90045-4

Papike, J.J., Spilde, M.N., Fowler, G.W., Layne, G.D., Shearer, C.K. (1995) The Lodran primitive achondrite: petrogenetic insights from electron and ion microprobe analysis of olivine and orthopyroxene. *Geochimica et Cosmochimica Acta* 59, 3061–3070. https://doi.org/10.1016/0016-7037(95)00195-6

Patzer, A., Hill, D.H., Boynton, W.V. (2004) Evolution and classification of acapulcoites and lodranites from a chemical point of view. *Meteoritics and Planetary Science* 39, 61–85. https://doi.org/10.1111/j.1945-5100.2004.tb00050.x

Stephant, A., Zhao, X., Anand, M., Davidson, J., Carli, C., Cuppone, T., Pratesi, G., Franchi, I.A. (2023) Hydrogen in acapulcoites and lodranites: A unique source of water for planetesimals in the inner Solar System, *Earth and Planetary Science Letters* 615, 118202. https://doi.org/10.1016/j.epsl.2023.118202

Tartèse, R., Anand, M., Joy, K.H., Franchi, I.A. (2014) H and Cl isotope systemat-ics of apatite in brecciated lunar meteorites Northwest Africa 4472, Northwest Africa 773, Sayh al Uhaymir 169, and Kalahari 009. *Meteoritics and Planetary Science* 49, 2266–2269. https://doi.org/10.1111/maps.12398

Yugami, K., Takeda, H., Kojima, H., Miyamoto, M. (1998) Modal mineral abundances and the differentiation trends in primitive achondrites. *Antarctic Meteorite Res*earch 11, 49–70.

Zipfel, J., Palme, H., Kennedy, A.K., Hutcheon, I.D. (1995) Chemical composition and origin of the Acapulco meteorite. *Geochimica et Cosmochimica Acta* 59, 3607–3627. https://doi.org/10.1016/0016-7037(95)00226-P